

Quantum Control beyond the Adiabatic Regime in 2D Curved Matter-Wave Guides

François Impens,¹ Romain Duboscq,² and David Guéry-Odelin³

¹*Instituto de Física, Universidade Federal do Rio de Janeiro, Rio de Janeiro, RJ 21941-972, Brazil*

²*Université de Toulouse; CNRS, INSA IMT, F-31062 Toulouse Cedex 9, France*

³*Laboratoire Collisions, Agrégats, Réactivité, IRSAMC, Université de Toulouse, CNRS, UPS, F-31062 Toulouse Cedex 09, France*



(Received 12 March 2020; accepted 4 June 2020; published 22 June 2020)

The propagation of matter waves in curved geometry is relevant for ion transport, atomtronics and electrons in nanowires. Curvature effects are usually addressed within the adiabatic limit and treated via an effective potential acting on the manifold to which the particles are strongly confined. However, the strength of the confinements that can be achieved experimentally are limited in practice, and the adiabatic approximation often appears too restrictive for realistic guides. Here, we work out a design method for 2D sharply bent waveguides beyond this approximation using an exact inverse-engineering technique. The efficiency of the method is confirmed by the resolution of the 2D nonlinear Schrödinger equation in curved geometry. In this way, we realize reflectionless and ultrarobust curved guides, even in the presence of interactions. Here, the transverse stability is improved by several orders of magnitude when compared to circular guides of similar size.

DOI: [10.1103/PhysRevLett.124.250403](https://doi.org/10.1103/PhysRevLett.124.250403)

Introduction.—The development of quantum technologies builds up on the increasing level of control of both internal and external degrees of freedom of atoms. This has motivated the design of quantum control protocols as key ingredients for such technologies. Quantum control protocols are mostly developed for quantum observables associated to flat coordinate systems. However, the geometry can drastically affect the quantum properties [1,2]: for instance, any kind of bending produces a bound state [3]. This suggests that geometry provides a powerful tool for controlling quantum systems. For instance, new forms of wave localization have been proposed by combining curved potentials and topological protection [4].

Since the pioneering works of Costa [1,2] and Goldstone and Jaffe [3] to establish the framework of quantum mechanics in curved geometry, the literature has focused on an effective 1D treatment relying on an adiabatic approximation [5–11]. In this approach, the effect of curvature is encapsulated in an effective attractive potential [3]. However, as explained below, the validity of quantum control protocols based on such a treatment is restricted to regimes of weak and slowly varying curvatures. Furthermore, many experimental situations such as electrons in quantum nanowires [12–17], propagation of atomic waves in guides [18], or the transfer of ions between different trap zones [19–23] often require going beyond this 1D approximation. In this Letter, we consider the real 2D problem and set up a nonadiabatic quantum control strategy valid in strongly curved geometry.

Such a study is relevant for the growing field of nanomaterials having complex geometries [12–14]. In the field of atomtronics, many techniques have been investigated to design guides [24–29]. The control of the external degrees of freedom

has also undergone an extraordinary progress with the realization of atom lasers having a high quality factor [30–37]. Guides with various shapes, including rings, have already been demonstrated for the development of guided matter-wave interferometry [24–29,38–44]. The applications and the miniaturization of matter-wave circuits require a perfect control of matter-wave propagation in a bent guide. A sharp bending favors compactness at the expense of a coupling between longitudinal and transverse degrees of freedom which may have deleterious consequences for the control of the matter wave [45–47]. The necessity of a perfect control in curved geometry is also an important prerequisite for setting up quantum computer platforms based on ions [19,20].

In the following, we first work out an inverse engineering strategy, inspired by shortcuts to adiabaticity (sta) protocols [48–50], to shape a class of classical trajectories robust to a variation in the initial conditions and free of residual transverse excitations after a bend. Then, we validate those solutions by a numerical resolution of the full 2D Schrödinger equation in curved space [51]. Our findings reveal how a proper guide design can dramatically reduce the transverse excitations after the bend, when compared to circular guides of identical radius and stiffness.

Schrödinger equation in curved geometry.—The coordinate of a material point using curvilinear coordinates (s, y) associated to a path $\mathbf{r}_c(s)$ are given by $\mathbf{r}(s, y) = \mathbf{r}_c(s) + y\mathbf{n}(s)$ where $\hat{\mathbf{n}}(s)$ is the local normal to the path. The variation with the curvilinear coordinate of the local normal vectors reads: $d\hat{\mathbf{t}}/ds = \kappa\hat{\mathbf{n}}$ and $d\mathbf{n}/ds = -\kappa\hat{\mathbf{t}}$ where $\hat{\mathbf{t}}(s) = d\mathbf{r}_c/ds$ is the local tangent and $\kappa(s) = 1/R(s)$ the local curvature.

The quantum mechanical wave function in curvilinear coordinates (s, y) can be written as $\psi(s, y) = h^{-1/2}(s, y)\tilde{\phi}(s, y)$. The complex-valued function $\tilde{\phi}(s, y)$ is given by a direct coordinate change in the cartesian coordinates wave function $\phi(X, Y)$: $\tilde{\phi}(s, y) = \phi[X(s, y), Y(s, y)]$ where $[X(s, y), Y(s, y)]$ are the cartesian coordinates associated to the classical point $\mathbf{r}(s, y)$ defined above. The factor $h^{-1/2}(s, y)$ arises from the Jacobian associated to the passage from cartesian to curvilinear coordinates. Indeed, the bending of the guide causes a local variation of the metric, captured by the definition of a function $h(s, y) = 1 - \kappa(s)y$ depending on the local path curvature $\kappa(s)$. Similar to general relativity, this inhomogeneous metric encodes the inertial forces. It is also responsible for the coupling between longitudinal and transverse degrees of freedom.

In its most general form, the curvilinear wave function $\psi(s, y)$ satisfies the following time-dependent Schrödinger equation in the presence of a transverse confining potential $V_{\perp}(y)$ [3]:

$$\left[-\frac{\hbar^2}{2m} \left(\frac{1}{h(s, y)} \frac{\partial}{\partial y} h(s, y) \frac{\partial}{\partial y} + \frac{1}{h(s, y)} \frac{\partial}{\partial s} \frac{1}{h(s, y)} \frac{\partial}{\partial s} \right) + V_{\perp}(y) \right] \psi(s, y) = i\hbar \frac{\partial \psi(s, y)}{\partial t}. \quad (1)$$

To recover the widely used adiabatic approximation, three criteria shall be fulfilled

$$(a) \sigma|\kappa| \ll 1, \quad (b) \sigma \left| \frac{d\kappa}{ds} \right| \ll \kappa, \quad (c) \sigma \left| \frac{d^2\kappa}{ds^2} \right| \ll \kappa^2, \quad (2)$$

where σ is the transverse size of the wave packet. In this limit, the Schrödinger equation becomes separable and yields independent longitudinal and transverse motions. Within the adiabatic approximation, the effect of curvature is encapsulated in an effective attractive 1D potential $V_{\text{eff}}(s) = -\hbar^2\kappa(s)^2/(8m)$, valid for sufficiently strong transverse confinement.

Our aim is to design the shape of a guide that connects two guides. To fix ideas, we consider a relative angle between the guides equal to $\alpha = 90^\circ$, the same transverse confinement for each guide, $V_{\perp}(y) = \frac{1}{2}m\omega^2y^2$, and an initial and final guide straight (see Fig. 1). The harmonic potential $V_{\perp}(y)$ is relevant for atomtronics and ion circuits, but also for GaN or ZnO based nanowires [57–60]. The generalization to initial and final wave guides having a finite curvature radius and/or for another relative angle is straightforward [61]. The simplest candidate is a quarter circle of constant radius R connecting the two straight guides. However, the abrupt change of curvature at the entrance and exit of such a bend generates a sudden centrifugal force that induces transverse excitations. To circumvent this limitation, in the following, we show how

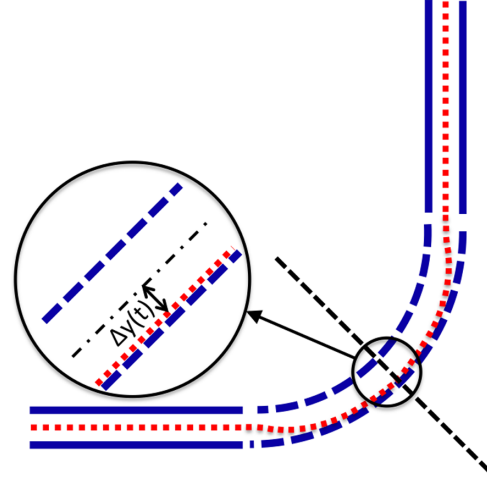


FIG. 1. Problem statement: How to connect two straight guides without inducing extra transverse oscillations in the output guide (trajectory represented by a dotted red line)?

to tailor the curvature profile $\kappa(s)$ as a function of the curvilinear coordinate s . At first sight, the direct solution of this problem through Eq. (1) seems very challenging. We overcome this difficulty by using a class of properly tailored classical solutions.

Exact inverse engineering.—The Newton law expressed in curvilinear coordinates yields

$$\ddot{s}(1 - \kappa y) - \dot{s}(\dot{\kappa}y + 2\kappa\dot{y}) = 0, \quad (3)$$

$$\ddot{y} + \omega^2y + \dot{s}^2\kappa(1 - \kappa y) = 0, \quad (4)$$

with $\kappa \equiv \kappa[s(t)]$. Combining Eqs. (3) and (4), we recover the conservation of energy

$$\dot{y}^2 + \omega^2y^2 + v_{\kappa}^2 = Cte = \frac{2E}{m}, \quad (5)$$

where $v_{\kappa} = \dot{s}(1 - \kappa y)$ [$\dot{v}_{\kappa} = \dot{s}\kappa\dot{y}$ from Eq. (3)]. The quantity $K_{\kappa}(\dot{s}, s, y) = \frac{1}{2}mv_{\kappa}^2$ is nothing but the longitudinal kinetic energy in a straight guide and, also, encapsulates the potential induced by inertial forces in a curved guide. An exact inverse engineering of the transverse motion is worked out by imposing the desired smooth trajectory for the transverse coordinates, $y(t)$. From Eq. (5), we then get $v_{\kappa}(t)$ from $y(t)$. This latter quantity gives access to both the longitudinal velocity from $\dot{s} = v_{\kappa} + \dot{s}\kappa y = v_{\kappa} + \dot{v}_{\kappa}y/\dot{y}$ and the time-dependent curvature at the particle position $\kappa[s(t)] = \dot{v}_{\kappa}(t)/[\dot{s}(t)\dot{y}(t)] = \dot{v}_{\kappa}/[d(v_{\kappa}y)/dt]$. The curvature profile $\kappa(s)$ is eventually reconstructed by integration of the longitudinal velocity [51].

For the connection between two orthogonal straight guides (see Fig. 1), we proceed in two symmetrical steps (dashed line at 45°). The connection is performed in a total time $2T$. To design the guide on the first segment of duration T , we impose the following boundary conditions:

$y_{\text{sta}}(0) = 0$, $y_{\text{sta}}(T) = \Delta y$, $\dot{y}_{\text{sta}}(0) = \dot{y}_{\text{sta}}(T) = 0$ and $\ddot{y}_{\text{sta}}(0) = \ddot{y}_{\text{sta}}(T) = 0$. The conditions at $t = 0$ translate the absence of transverse excitation at the entrance of the bend. The conditions at $t = T$ are required for two reasons: it ensures the continuity of the position and velocity in the middle of the guide, and it enforces the stability of the trajectory against the final time $2T$. As such, it improves the resilience against a small dispersion in the longitudinal velocity [50]. This latter requirement is relevant for the propagation of a matter wave since the wave packet has finite size and, thus, a finite velocity dispersion. To accommodate for the boundary conditions, we choose a trajectory in the form of a polynomial $y_{\text{sta}}(t) = P(t/T)$ with $P(x) = \Delta y(10x^3 - 15x^4 + 6x^5)$. Many other choices could be made for this interpolating function depending on the relevant constraints as discussed in [61,62].

The free parameter Δy is fixed by the choice of the maximum curvature, κ_m , reached at $t = T$: $\Delta y = -\frac{1}{4}\kappa_m^{-1}(\sqrt{1 + 8\dot{s}(T)^2\kappa_m^2/\omega^2} - 1)$. The time T is determined self-consistently by the choice of the rotation angle $\alpha' = \langle \hat{\mathbf{t}}[s(0)], \hat{\mathbf{t}}[s(T)] \rangle = \int_0^T dt \kappa[s(t)]\dot{s}(t)$ ($\alpha' = \pi/4$ for our example)

$$\alpha' = - \int_0^T dt \frac{\ddot{y}_{\text{sta}}(t) + \omega^2 y_{\text{sta}}(t)}{\sqrt{2E/m - \dot{y}_{\text{sta}}^2(t) - \omega^2 y_{\text{sta}}^2(t)}}. \quad (6)$$

By symmetry, the solution for $T \leq t \leq 2T$ reads: $y_{\text{sta}}(t) = P(1 - t/T)$.

To quantify the compactness of the tailored bend, we define the effective radius of curvature R_{eq} as the radius of the largest quarter circle enclosed within the engineered bend. Figure 2(a) gives an example of an engineered curvature profile with $R_{\text{eq}} = 10 \mu\text{m}$ for typical experimental parameters $\dot{s}_0 = 20 \text{ mm/s}$ and $\omega/2\pi = 1705 \text{ Hz}$ [55]. Figure 2(b) shows the engineered bend together with the effective radius of curvature R_{eq} .

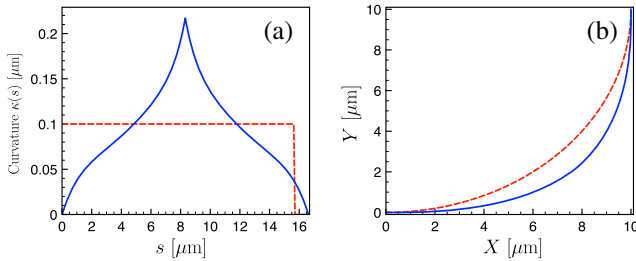


FIG. 2. (a) Inverse-engineered curvature profile $\kappa(s)$ (solid blue line) and the corresponding effective circular bend of radius $R_{\text{eq}} = 10 \mu\text{m}$ (red dashed line) as a function of the longitudinal coordinate s . (b) View from above of the inverse-engineered path (blue) shape and of the equivalent circular path (red). Parameters: initial longitudinal velocity of $\dot{s}_0 = 20 \text{ mm/s}$, trapping frequency $\omega = 2\pi \times 1705 \text{ Hz}$, and a maximum curvature $\kappa_m = 0.22 \mu\text{m}^{-1}$. The total length is $s_f \approx 16.6 \mu\text{m}$ corresponding to a total time $2T \approx 0.88 \text{ ms}$.

Robust cancellation of the transverse excitations.—For a bend defined by a quarter circle, the curvature is a step function that drives transverse oscillations that generally persist beyond the bend. Their amplitude depends on the particle parameters at the entrance of the guide and on the phase of the transverse oscillation at the exit of the bend. As a result, there exists a set of discrete radius values for which there is an exact cancellation of the oscillations of the outgoing particle [45,55].

Nevertheless, even in these most favorable circumstances, it turns out that the 2D inverse-engineered guide outperforms the circular path when one considers the average transverse stabilization achieved over a finite velocity interval. As already explained above, a desirable feature of a matter wave guide is, indeed, to suppress transverse excitations over a finite range of longitudinal velocities and not only for isolated values. To quantify the robustness of the guide, we consider a uniform distribution of initial velocities over the interval $[(1 - \epsilon)\dot{s}_0, (1 + \epsilon)\dot{s}_0]$, where \dot{s}_0 is the incident longitudinal velocity used in the inverse-engineering procedure and with $\epsilon = 5\%$. Each initial velocity v yields oscillations at the exit of the bend of finite amplitude $a_c(v)$ and $a_{\text{sta}}(v)$ for the circular and the inverse-engineered guide, respectively. We measure the robustness by computing the dimensionless quantities $\bar{\alpha}_{c,\text{sta}} = (2\epsilon\dot{s}_0\sigma)^{-1} \int_{\dot{s}_0-\epsilon}^{\dot{s}_0+\epsilon} a_{c,\text{sta}}(v)dv$, corresponding to the ratio between the averaged oscillation amplitudes and the width $\sigma = \sqrt{\hbar/m\omega}$ of the transverse ground state wave function. For an oscillation amplitude a , the outgoing particle has a transverse mechanical energy E which compares to the energy quantum as $E/\hbar\omega = \frac{1}{2}(a/\sigma)^2$. Figure 3 shows the oscillation amplitudes $\bar{\alpha}_{c,\text{sta}}$ as a function of the effective radius. The engineered guide yields transverse excitations that are at least 1 order of magnitude (and for some radii more than 2 orders of magnitude) smaller than that of the circular guide.

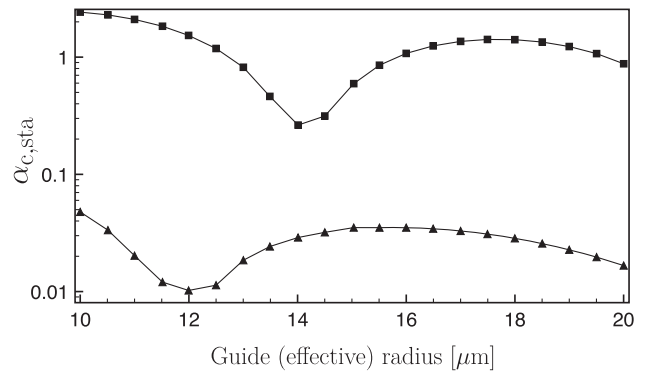


FIG. 3. Averaged oscillation amplitudes $\bar{\alpha}_{\text{sta}}$ for the engineered guides (triangle) and $\bar{\alpha}_c$ for the circular guides (square) after a right turn as a function of the guide radius. Same initial longitudinal velocity and trapping frequency as for Fig. 2.

Comparison between 2D and 1D curvature designs.—To facilitate the comparison between our 2D treatment and the 1D effective approach [5–11], we define in the following manner the 1D-adiabatic design.

The adiabatic limit yields an independent longitudinal motion driven by an attractive bending potential $V_{\text{eff}}(s)$. Thus, the longitudinal velocity is expected to increase with the local curvature as $\dot{s}_{cl} = \sqrt{\dot{s}_0^2 - 2V_{\text{eff}}(s_{cl})/m}$ with \dot{s}_0 the longitudinal velocity of the atomic wave packet before the bend. From the classical equation (4), we infer the expression of the curvature $\kappa_{1D}(s)$ as a function of the transverse trajectory $y_{\text{sta}}(t)$ defined previously with $T = T_{1D}$ whose value is determined by the desired rotation angle $\pi/4 = \int_0^{T_{1D}} dt \dot{s}_{cl}(t) \kappa_{1D}(s_{cl}(t))$. We use this determination of the curvature in 2D simulations performed either with classical or Schrödinger equations.

The 2D-curvature design is obtained from the procedure explained in the previous section. It relies on a similar transverse trajectory $y_{\text{sta}}(t)$ but defined with the time T_{2D} to get the desired angle [see (6)].

Here, we work out a concrete example with the parameters: $\dot{s}_0 = 20$ mm/s and $\omega = 2\pi \times 1705$ Hz. We find $T_{1D} = 0.334$ ms for $\kappa_{1D}(s)$ and $T_{2D} = 0.295$ ms for $\kappa_{2D}(s)$, corresponding to the respective bend lengths $s_{f1D} = 13.36$ μm and $s_{f2D} = 10.37$ μm , and to the effective radii of curvature $R_{\text{eq}2D} = 8.37$ μm and $R_{\text{eq}1D} = 6.47$ μm . The initial wave function is a cigar-shaped Gaussian wave function of widths $\sigma_y = \sigma_s/10 = (\hbar/m\omega)^{1/2}$ initially centered on the axis $y = 0$, at the normalized longitudinal position $s/s_f = -0.5$ and with an average velocity \dot{s}_0 (see Fig. 4). With this initial position, the wave packet is at $t = 0$ entirely outside the bend.

The effectiveness of the two methods is analyzed through both the classical 2D Newton equations and the numerical resolution of the full 2D Schrödinger equation (1) for both curvature profiles $\kappa_{1D}(s)$ and $\kappa_{2D}(s)$ [51]. The results are summarized in Fig. 4 where the transverse position and longitudinal velocities of the packet are plotted as a function of the normalized longitudinal coordinate s/s_f for both curvature designs.

For our choice of parameters, the curvature $\kappa(s)$ varies considerably on the width of the wave packet as $\sigma_s/s_f \sim 0.2$ for both guides. This contributes to the clear difference between the classical (dotted-dashed lines) and quantum trajectories (solid lines). With the 1D adiabatic-design bend, we observe strong transverse oscillations that persist in the output straight guide ($s/s_f \geq 1$) [see Fig. 4(a)]. Therefore, this design fails to provide a reliable connection between the two straight guides for both classical and quantum simulations. A totally different behavior is obtained with the 2D-curvature design: the transverse oscillations in the output channel are almost completely suppressed. As a figure of merit, for each guide, we evaluate the exceeding transverse energy of the wave

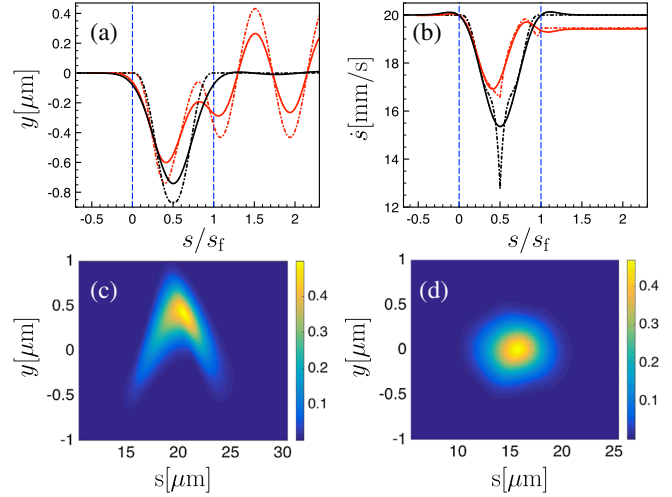


FIG. 4. (a) and (b): Transverse position, $\langle y(s/s_f) \rangle$, and longitudinal velocity, $\langle \dot{s} \rangle(s/s_f)$, of the wave packet as a function of the normalized longitudinal coordinate, s/s_f . The curves are obtained from 2D classical simulations using either the 1D-adiabatic design (red dotted-dashed line) or the 2D-optimized protocol (black dotted-dashed line), or from the 2D Schrödinger equation (1) using either the 1D-adiabatic design (red solid line) or the 2D-optimized protocol (black solid line). Color plot of the modulus square of the 2D wave function $|\phi(s, y)|^2$ (in μm^{-2}) after propagation at the position $s = 1.5s_f$ for the 1D-adiabatic design (c) and 2D-nonadiabatic design (d). Parameters: initial Gaussian wave function of widths $\sigma_y = \sigma_s/10 = (\hbar/m\omega)^{1/2}$ centered on axis ($y = 0$) at $s = -0.5s_f$ and with a velocity $\dot{s}_0 = 20$ mm/s.

packet once in the output straight guide with respect to the ground state energy scale $\Delta E_t = \langle \frac{1}{2} p_y^2/m + \frac{1}{2} m\omega^2 y^2 \rangle - \frac{1}{2} \hbar\omega = \bar{n}\hbar\omega$. We obtain the respective average number of transverse excitations quanta $\bar{n}_{1D} = 1.4$ and $\bar{n}_{2D} = 5.1 \times 10^{-3}$ for the 1D-adiabatic and 2D designs, respectively. With our 2D protocol, we reach a fidelity up to 99.6%. These results validate our strategy.

Figure 4(b) shows the evolution of the longitudinal velocity along the bend for both guides. For the 1D guide, the final longitudinal velocity obtained from quantum simulations is noticeably below its initial value, which witnesses the transfer of energy between the longitudinal and transverse degrees of freedom. A common feature of both bent guides is that the longitudinal velocity significantly decreases when the wave packet is expelled from the bend center. This is a fingerprint of angular momentum conservation, even though with the considered position-dependent curvature profile angular momentum is not rigorously conserved. This correlation is a signature that the propagation occurs beyond the adiabatic regime, for which the longitudinal and transverse motion are expected to be independent [3,5–11]. It is remarkable that the longitudinal velocity obtained from the 2D Schrödinger equation is, indeed, minimal in the region of strong curvature, where it should be maximal according to the

1D adiabatic approach. This suggests that the convergence of the longitudinal velocity profile towards the adiabatic limit is slow. Indeed, the considered 2D curvature profile $\kappa_{2D}(s)$ presents rapid variations which violate the adiabatic criteria (2)(b) and (2)(c), as $\sigma|d\kappa_{2D}/ds| \simeq 0.6\kappa$ and $\sigma|d^2\kappa_{2D}/ds^2| \simeq 5\kappa^2$ in the vicinity of the strongly curved region of the bend. In this regime, our procedure clearly outperforms previous methods based on an effective 1D potential. Our method only breaks down when the condition (2)(a) is violated. Indeed, in this extreme limit, the classical-quantum correspondence fails down since the inertial force strongly varies over the wave packet size.

Interestingly, our design protocol remains valid in the presence of interactions (see [51]). Over a wide range of nonlinear couplings g_{2D} well beyond the perturbative regime ($-0.95 < g_{2D}/g_0 < 0.75$ with $g_0/m = 1 \mu\text{m}^4 \text{m s}^{-2}$), the quantum fidelity remains larger than 99% when we compare the propagation in the curved guide [same parameter as for Fig. 4(d)] with that in a straight guide for the same propagation time. We have propagated matter-wave solitons [56,63] and found a regime of interactions ($-0.5 < g_{2D}/g_0 < 0$) with a fidelity almost equal to the interaction-free value. This extra robustness is attributed to the quasiparticle behavior of solitons.

To conclude, we have presented a systematic procedure to design reflectionless strongly curved 2D matter wave guides with unprecedented quantum fidelity. Our study has also revealed the pitfalls of 1D effective potential, and the very slow convergence of a real system towards this type of adiabatic limit. Our approach provides a new strategy for quantum control in curved geometry beyond the adiabatic regime and is a step forward towards the realization of highly stable complex matter wave circuits and of a portable guided matter-wave interferometer [18,24–29, 39–44,55,64] including solitons [65].

We thank Xavier Marie, Xavier Bouju, and Rodrigo B. Capaz for their useful comments about the manuscript. This work is part of INCT-IQ from CNPq. It was supported by the Brazilian agencies CNPq (Grant Universal No. 409994/2018-9), CAPES, and FAPERJ (Grant APQ1 No. 210.296/2019) and the Agence Nationale de la Recherche research funding Grant No. ANR-18-CE30-0013.

[1] R. C. T. da Costa, *Phys. Rev. A* **23**, 1982 (1981).
 [2] R. C. T. da Costa, *Phys. Rev. A* **25**, 2893 (1982).
 [3] J. Goldstone and R. L. Jaffe, *Phys. Rev. B* **45**, 14100 (1992).
 [4] C.-Y. Lin, G. Marcucci, G. Wang, Y.-L. Chuang, C. Conti, and R.-K. Lee, *arXiv:2002.03091*.
 [5] I. J. Clark and A. J. Bracken, *J. Phys. A* **29**, 4527 (1996).
 [6] G. Cantele, D. Ninno, and G. Iadonisi, *Phys. Rev. B* **61**, 13730 (2000).
 [7] P. Leboeuf and N. Pavloff, *Phys. Rev. A* **64**, 033602 (2001).

[8] X. Duan, C. Niu, V. Sahi, J. Chen, J. W. Parce, S. Empedocles, and J. L. Goldman, *Nature (London)* **425**, 274 (2003).
 [9] A. del Campo, M. G. Boshier, and A. Saxena, *Sci. Rep.* **4**, 5274 (2015).
 [10] P. Grivickas, J. F. Geisz, and Y. M. Gupta, *Appl. Phys. Lett.* **113**, 072101 (2018).
 [11] C. Schindler, C. Wiegand, J. Sichau, L. Tiemann, K. Nielsch, R. Zierold, and R. H. Blick, *Appl. Phys. Lett.* **111**, 171601 (2017).
 [12] H. Shima, M. Sato, K. Iiboshi, S. Ghosh, and M. Arroyo, *Phys. Rev. B* **82**, 085401 (2010); B. Novakovic, R. Akis, and I. Knezevic, *Phys. Rev. B* **84**, 195419 (2011); F. Santos, S. Fumeron, B. Berche, and F. Moraes, *Nanotechnology* **27**, 135302 (2016).
 [13] C. Ortix and J. van den Brink, *Phys. Rev. B* **81**, 165419 (2010).
 [14] S. Tanda, T. Tsuneta, Y. Okajima, K. Inagaki, K. Yamaya, and N. Hatakenaka, *Nature (London)* **417**, 397 (2002); J. Gravesen, M. Willatzen, and L. C. L. Y. Voon, *J. Math. Phys. (N.Y.)* **46**, 012107 (2005).
 [15] A. V. Zampetaki, J. Stockhofe, S. Krönke, and P. Schmelcher, *Phys. Rev. E* **88**, 043202 (2013).
 [16] T. Thitapura, W. Liewrian, T. Jutarosaga, and S. Boonchui, *Plasmonics* **12**, 1439 (2017).
 [17] R. Cheng, Y.-L. Wang, H.-X. Gao, H. Zhao, J.-Q. Wang, and H.-S. Zong, *J. Phys. Condens. Matter* **32**, 025504 (2020).
 [18] L. Amico, G. Birkl, M. Boshier, and L.-C. Kwek, *New J. Phys.* **19**, 020201 (2017).
 [19] D. Kielpinski, C. Monroe, and D. J. Wineland, *Nature (London)* **417**, 709 (2002).
 [20] J. P. Home, D. Hanneke, J. D. Jost, J. M. Amini, D. Leibfried, and D. J. Wineland, *Science* **325**, 1227 (2009).
 [21] R. Bowler, J. Gaebler, Y. Lin, T. R. Tan, D. Hanneke, J. D. Jost, J. P. Home, D. Leibfried, and D. J. Wineland, *Phys. Rev. Lett.* **109**, 080502 (2012).
 [22] A. Walther, F. Ziesel, T. Ruster, S. T. Dawkins, K. Ott, M. Hettrich, K. Singer, F. Schmidt-Kaler, and U. Poschinger, *Phys. Rev. Lett.* **109**, 080501 (2012).
 [23] S. An, D. Lv, A. del Campo, and K. Kim, *Nat. Commun.* **7**, 12999 (2016).
 [24] S. Wu, W. Rooijackers, P. Striehl, and M. Prentiss, *Phys. Rev. A* **70**, 013409 (2004).
 [25] O. Morizot, Y. Colombe, V. Lorent, H. Perrin, and B. M. Garraway, *Phys. Rev. A* **74**, 023617 (2006).
 [26] B. E. Sherlock, M. Gildemeister, E. Owen, E. Nugent, and C. J. Foot, *Phys. Rev. A* **83**, 043408 (2011).
 [27] J. D. Pritchard, A. N. Dinkelaker, A. S. Arnold, P. F. Griffin, and E. Riis, *New J. Phys.* **14**, 103047 (2012).
 [28] S. Moulder, S. Beattie, R. P. Smith, N. Tammuz, and Z. Hadzibabic, *Phys. Rev. A* **86**, 013629 (2012).
 [29] I. Lesanovsky and W. von Klitzing, *Phys. Rev. Lett.* **99**, 083001 (2007).
 [30] A. E. Leanhardt, A. P. Chikkatur, D. Kielpinski, Y. Shin, T. L. Gustavson, W. Ketterle, and D. E. Pritchard, *Phys. Rev. Lett.* **89**, 040401 (2002).
 [31] W. Guerin, J.-F. Riou, J. P. Gaebler, V. Josse, P. Bouyer, and A. Aspect, *Phys. Rev. Lett.* **97**, 200402 (2006).

- [32] J.-F. Riou, W. Guerin, Y. Le Coq, M. Fauquembergue, V. Josse, P. Bouyer, and A. Aspect, *Phys. Rev. Lett.* **96**, 070404 (2006).
- [33] A. Couvert, M. Jeppesen, T. Kawalec, G. Reinaudi, R. Mathevet, and D. Guéry-Odelin, *Europhys. Lett.* **83**, 50001 (2008).
- [34] F. Impens, *Phys. Rev. A* **77**, 013619 (2008).
- [35] F. Impens, *Phys. Rev. A* **80**, 063617 (2009).
- [36] M. Johnsson, S. Haine, J. Hope, N. Robins, C. Figl, M. Jeppesen, J. Dugue, and J. Close, *Phys. Rev. A* **75**, 043618 (2007).
- [37] G. L. Gattobigio, A. Couvert, M. Jeppesen, R. Mathevet, and D. Guéry-Odelin, *Phys. Rev. A* **80**, 041605(R) (2009).
- [38] C. J. Bordé, *Phys. Lett.* **140A**, 10 (1989).
- [39] S. Eckel, J. G. Lee, F. Jendrzejewski, N. Murray, C. W. Clark, C. J. Lobb, W. D. Phillips, M. Edwards, and G. K. Campbell, *Nature (London)* **506**, 200 (2014).
- [40] T. A. Bell, J. A. P. Glidden, L. Humbert, M. W. J. Bromley, S. A. Haine, M. J. Davis, T. W. Neely, M. A. Baker, and H. Rubinsztein-Dunlop, *New J. Phys.* **18**, 035003 (2016).
- [41] S. Pandey, H. Mas, G. Drougakis, P. Thekkeppatt, V. Bolpasi, G. Vasilakis, K. Poullos, and W. von Klitzing, *Nature (London)* **570**, 205 (2019).
- [42] Y. Guo, R. Dubessy, M. G. de Herve, A. Kumar, T. Badr, A. Perrin, L. Longchambon, and H. Perrin, *Phys. Rev. Lett.* **124**, 025301 (2020).
- [43] W. Hänsel, P. Hommelhoff, T. W. Hänsch, and J. Reichel, *Nature (London)* **413**, 498 (2001).
- [44] D. Müller, D. Z. Anderson, R. J. Grow, P. D. D. Schwindt, and E. A. Cornell, *Phys. Rev. Lett.* **83**, 5194 (1999).
- [45] M. W. J. Bromley and B. D. Esry, *Phys. Rev. A* **69**, 053620 (2004).
- [46] G. L. Gattobigio, A. Couvert, B. Georgeot, and D. Guéry-Odelin, *Phys. Rev. Lett.* **107**, 254104 (2011).
- [47] G. L. Gattobigio, A. Couvert, G. Reinaudi, B. Georgeot, and D. Guéry-Odelin, *Phys. Rev. Lett.* **109**, 030403 (2012).
- [48] R. Corgier, S. Amri, W. Herr, H. Ahlers, J. Rudolph, Guéry-Odelin, E. M. Rasel, E. Charron, and N. Gaaloul, *New J. Phys.* **20**, 055002 (2018).
- [49] F. Impens and D. Guéry-Odelin, *Sci. Rep.* **9**, 4048 (2019).
- [50] D. Guéry-Odelin, A. Ruschhaupt, A. Kiely, E. Torrontegui, S. Martínez-Garaot, and J. G. Muga, *Rev. Mod. Phys.* **91**, 045001 (2019).
- [51] See Supplemental Material at <http://link.aps.org/supplemental/10.1103/PhysRevLett.124.250403> for additional details on the inverse-engineering procedure, the current state-of-the-art in atomtronics and the quantitative study in the presence of interactions, which includes Refs. [9,45,52–56].
- [52] C. Chin, R. Grimm, P. Julienne, and E. Tiesinga, *Rev. Mod. Phys.* **82**, 1225 (2010).
- [53] K. E. Strecker, G. B. Partridge, A. G. Truscott, and R. G. Hulet, *Nature (London)* **417**, 150 (2002).
- [54] C. Besse, *C.R. Acad. Sci. Ser. I* **326**, 1427 (1998).
- [55] C. Ryu and M. G. Boshier, *New J. Phys.* **17**, 092002 (2015).
- [56] L. Khaykovich, F. Schreck, G. Ferrari, T. Bourdel, J. Cubizolles, L. D. Carr, Y. Castin, and C. Salomon, *Science* **296**, 1290 (2002); K. E. Strecker, G. B. Partridge, A. G. Truscott, and R. G. Hulet, *Nature (London)* **417**, 150 (2002).
- [57] E. A. Laird, F. Kuemmeth, G. A. Steele, K. Grove-Rasmussen, J. Nygard, K. Flensberg, and L. P. Kouwenhoven, *Rev. Mod. Phys.* **87**, 703 (2015).
- [58] G. Santoruvo, A. Allain, D. Ovchinnikov, and E. Matioli, *Appl. Phys. Lett.* **109**, 103102 (2016).
- [59] S. Bagga, J. Akhtar, and S. Mishra, *AIP Conf. Proc.* **1989**, 020004 (2018).
- [60] M. A. Johar, H.-G. Song, A. Waseem, M. A. Hassan, I. V. Bagal, Y.-H. Cho, and S.-W. Ryu, *Appl. Mater. Today* **19**, 100541 (2020).
- [61] D. Guéry-Odelin and J. G. Muga, *Phys. Rev. A* **90**, 063425 (2014).
- [62] V. Martikyan, D. Guéry-Odelin, and D. Sugny, *Phys. Rev. A* **101**, 013423 (2020).
- [63] V. M. Pérez-García, H. Michinel, and H. Herrero, *Phys. Rev. A* **57**, 3837 (1998).
- [64] E. R. Moan, R. A. Horne, T. Arpornthip, Z. Luo, A. J. Fallon, S. J. Berl, and C. A. Sackett, *Phys. Rev. Lett.* **124**, 120403 (2020).
- [65] G. D. McDonald, C. C. N. Kuhn, K. S. Hardman, S. Bennetts, P. J. Everitt, P. A. Altin, J. E. Debs, J. D. Close, and N. P. Robins, *Phys. Rev. Lett.* **113**, 013002 (2014).